


## Article

# Phase Transformation Kinetics of a FCC $\text{Al}_{0.25}\text{CoCrFeNi}$ High-Entropy Alloy during Isochronal Heating

Jun Wang , Chen Wei, Haoxue Yang, Tong Guo, Tingting Xu and Jinshan Li

State Key Laboratory of Solidification Processing, Northwestern Polytechnical University, Xi'an 710072, Shaanxi, China; 18229022561@163.com (C.W.); anlylin@163.com (H.Y.); believevt@163.com (T.G.); m18165310761\_1@163.com (T.X.); ljsh@nwpu.edu.cn (J.L.)

\* Correspondence: nwpuwj@nwpu.edu.cn; Tel.: +86-29-8846-0568; Fax: +86-29-8846-0294

Received: 6 November 2018; Accepted: 29 November 2018; Published: 3 December 2018



**Abstract:** The phase transformation kinetics of a face-centered-cubic (FCC)  $\text{Al}_{0.25}\text{CoCrFeNi}$  high-entropy alloy during isochronal heating is investigated by thermal dilation experiment. The phase transformed volume fraction is determined from the thermal expansion curve, and results show that the phase transition is controlled by diffusion controlled nucleation-growth mechanism. The kinetic parameters, activation energy and kinetic exponent are determined based on Kissinger–Akahira–Sunose (KAS) and Johnson–Mehl–Avrami (JMA) method, respectively. The activation energy and kinetic exponent determined are almost constant, indicating a stable and slow speed of phase transition in the FCC  $\text{Al}_{0.25}\text{CoCrFeNi}$  high-entropy alloy. During the main transformation process, the kinetic exponent shows that the phase transition is diffusion controlled process without nucleation during the transformation.

**Keywords:** high-entropy alloy; phase transformation; kinetics; isochronal heating

## 1. Introduction

High-entropy alloys (HEAs) have attracted extensive attention as its unique designing philosophy and excellent comprehensive properties such as high strength, high toughness and good corrosion resistance [1–5]. Tuning the microstructure and improving the mechanical properties have been one of the most interesting fields for many researchers. Heat treatment is widely used for many kinds of materials in order to obtain ideal integrated properties effectively without macro appearance destruction. Implementation of heat treatment to high-entropy alloys also achieved many successful cases [6–11]. For example, Niu et al. [12] studied the tensile properties of  $\text{Al}_{0.5}\text{CoCrFeNi}$  HEAs annealed at 650 °C and found the alloy is highly strengthened by nanoprecipitations. Munitz et al. [8] studied the effect of heat treatment on the microstructure and mechanical properties of  $\text{AlCoCrFeNi}$  HEAs, and found that the formation of brittle  $\sigma$  phase heat treated at 850 °C caused micro-hardness of the inter-dendrite region increasing dramatically and the dissolution of  $\sigma$  phase at 975 °C induced alloy softening.

The heat treatment is solid state phase transformation which is usually described by thermodynamics as well as kinetics [13]. Kinetics way of tailoring phases is significantly important for HEAs to obtain outstanding integrated performance.  $\text{Al}_x\text{CoCrFeNi}$  ( $0 \leq x \leq 1$ ) HEAs are one of the most commonly investigated alloys that owns very good properties and easily to be tunable by changing the Al content, heat treatment and forging [14–23].

In our previous research, the phase transformation kinetics of  $\text{Al}_{0.5}\text{CoCrFeNi}$  HEA was inspected and reasonable heat treatment parameters were found [24]. Overall, kinetics analysis is absolutely important for high-entropy alloys to realize tuning microstructure and properties. Yet the research in

this field is insufficient and further study is needed. In this paper, the phase transformation kinetics of a face-centered-cubic (FCC)  $\text{Al}_{0.25}\text{CoCrFeNi}$  high-entropy alloy is analyzed by thermal dilation experiment to learn the phase transition mechanism.

## 2. Experimental Procedures

Al, Co, Cr, Fe, and Ni with high purities ( $\geq 99.95$  wt. %) were used to prepare  $\text{Al}_{0.25}\text{CoCrFeNi}$  high-entropy alloy ingots by arc-melting under inert (argon) atmosphere. Each ingot was re-melted at least four times so as to achieve homogeneity. The exact composition of the ingot checked by energy dispersive X-ray spectrometry (EDS, JEOL, JSM-6390, Tokyo, Japan) analysis (the errors for each element is less than  $\pm 5\%$ ) is  $\text{Al}_{5.7}\text{Co}_{23.4}\text{Cr}_{22.8}\text{Fe}_{23.5}\text{Ni}_{24.6}$ .

After polishing and clean with ethanol, the ingots were casted into rods with dimension of  $\phi 6 \times 70$  mm. The rods were machined into specimens with dimension of  $\phi 6 \times 25$  mm. Then the rods directly taken from the as-cast alloy are used for thermal dilation test by Netzsch®DIL-402C (Selb, Germany). The tests were carried out under the protection of argon and the heating rates in this paper are 4 K/min, 6 K/min, 8 K/min and 10 K/min, respectively. The microstructure and phases were characterized by X-ray diffractometer (XRD, DX 2700, Dandong, China) and scanning electron microscope (JEOL, JSM-6390, Tokyo, Japan), respectively.

## 3. Results

### 3.1. Thermal Expansion Curve

Figure 1a shows the thermal dilation curve of  $\text{Al}_{0.25}\text{CoCrFeNi}$  HEA measured at heating rate of 4 K/min and Figure 1b is the differential curve of Figure 1a. As is shown in Figure 1b, two phase transition can be pointed from the differential curve. The starting temperatures for these two phase transition are 760 K and 995 K, which are determined to be the FCC-L1<sub>2</sub> and FCC-B2 phase transition [25], respectively. According to the thermal expansion curve, the first transition FCC-L1<sub>2</sub> shows a much larger thermal expansion behavior, which will be investigated in detail below.

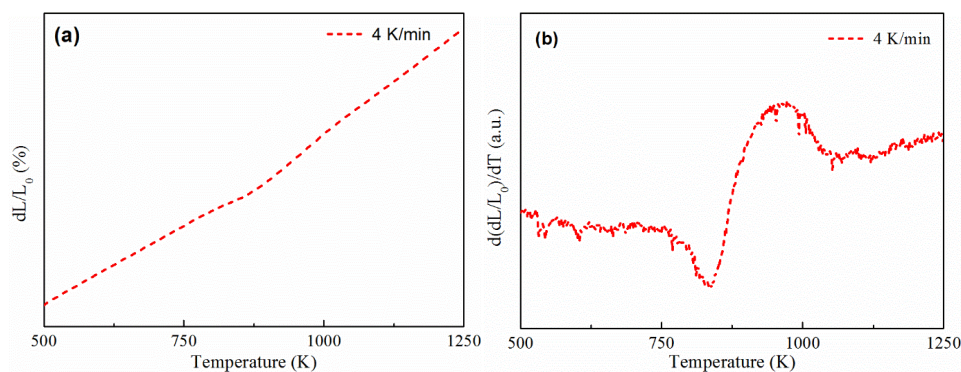


**Figure 1.** (a) The thermal dilation curve of  $\text{Al}_{0.25}\text{CoCrFeNi}$  high-entropy alloy measured at 4 K/min heating rate, and (b) the differential of the thermal dilation curve.

### 3.2. Determination of Phase Transformed Volume

The thermal dilation curves of  $\text{Al}_{0.25}\text{CoCrFeNi}$  HEA measured at different heating rates are presented in Figure 2a. All the curves exhibit the same variation tendency, indicating good repeatability of the thermal dilation experiment. As to the FCC-L1<sub>2</sub> phase transition, the phase transformed volume can be calculated by the lever rule method [26–28]. Taking the specimen measured at 4 K/min as an example, specific lever rule method explanation is shown in Figure 2b. The lines AA' and BB' can be gained by extending the linear expansion stage before and after the phase transition. After connecting the A' and B', the point intersection of A'B' and the thermal dilation curve is C. Then, the phase transition volume fraction at specific temperature can be calculated by Equation (1).

$$f(x) = \frac{y_{A'} - y_C}{y_{A'} - y_{B'}} \quad (1)$$

where  $f$  is the phase transition volume fraction and  $y_{A'}$ ,  $y_{B'}$ ,  $y_C$  are the Y-axis values of  $A'$ ,  $B'$  and  $C$ , respectively. All the thermal dilation curves in Figure 2a are analyzed by the recommended lever rule method and the result is shown in Figure 3.

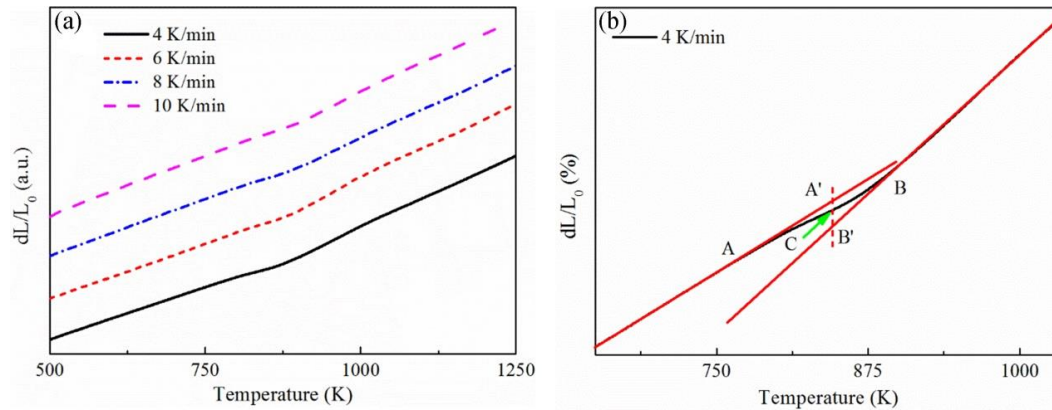


**Figure 2.** (a) The thermal dilation curves of  $\text{Al}_{0.25}\text{CoCrFeNi}$  HEA measured at different heating rates and (b) an example of calculating  $f$  by level ruler method. The red lines are used for determine the starting (A) and ending (B) point of the phase transition, and the intersection (C) of the dashed line and the thermal expansion curve is used for the calculation of  $f$  using Equation (1).

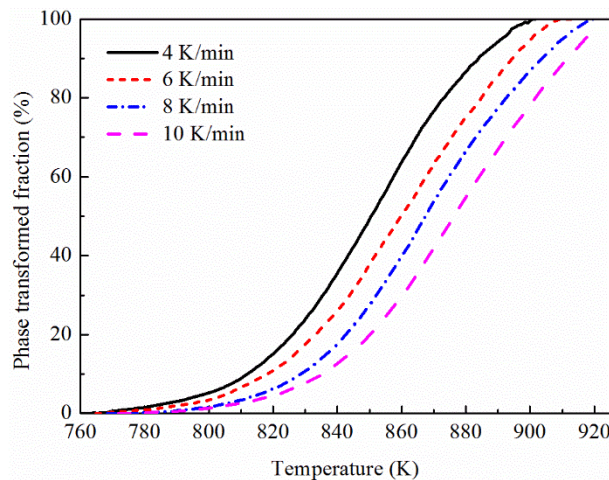


**Figure 3.** Phase transformed volume as a function of temperature of  $\text{Al}_{0.25}\text{CoCrFeNi}$  high-entropy alloy measured at different heating rates.

The phase transformed fraction ( $f$ ) as a function of temperature at different heating rates are shown in Figure 3. At the starting period of phase transition (when  $f < 10\%$ ), the slope of the curves are very small, illustrating the slowly phase transition rate. The slope of curves gets bigger gradually with the continuous increasing of temperature which means the phase transition becomes faster. Overall, the whole transition curves present a “S” shape, which is a proof that the FCC-L1<sub>2</sub> phase transition is controlled by the nucleation-growth mechanism [27].

### 3.3. Calculation of Activation Energy

Activation energy ( $E$ ) is a significant thermodynamic parameter for the evaluation of phase transition barrier. The activation energy of FCC-L1<sub>2</sub> phase transition in  $\text{Al}_{0.25}\text{CoCrFeNi}$  HEA would change with the variation of local chemical composition at different stages of phase transition. So the

apparent activation energy obtained by considering the activation energy at each stage of phase transition is used to assess the transition process. There are many methods that can calculate the activation energy during solid state phase transition, and the generalized Kissinger method (also called Kissinger-Akahira-Sunose (KAS) method) [29] is a well-known one that is very efficient and accurate. The method using the following equation:

$$\ln\left(\frac{T^2}{\Phi}\right) = -C + \frac{E}{RT} \quad (2)$$

where  $T$  is temperature at certain transformed volume,  $\Phi$  is the heating rate,  $C$  is a constant and  $R$  is the molar gas constant. Specific values of  $T$  and  $\Phi$  can be gained from the phase transformed fraction curves shown in Figure 3. Linear regression between  $\ln(T^2/\Phi)$  and  $1/T$  ( $1/T$  is replaced by  $10,000/T$  in order to simplify the calculation) is obtained by calculation of Equation (2) with the temperature corresponding to different heating rates (4 K/min, 6 K/min, 8 K/min, 10 K/min) and using  $T$  at four different transformed volume fraction: 0.2, 0.4, 0.6 and 0.8 (in fact, when  $f$  is close to 0 or 1, there will be a large error for the calculation due to the error caused during determination of  $f$ ). The linear regression results are exhibited in Figure 4 and the slope of each line represents the value of  $E/R$  for the corresponding phase transformed fraction. The determined activation energies are shown in Figure 5. There is a decreasing tendency of the activation energy with the increasing transformed volume, however, the difference is quite small and the value is around  $198 \pm 1$  kJ/mol.

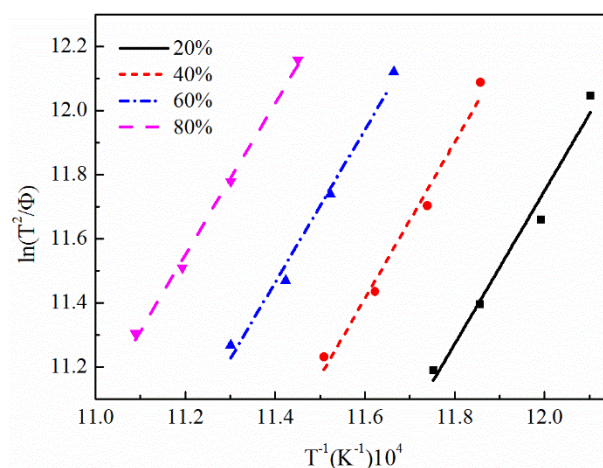


**Figure 4.** The KAS plot of  $10,000/T \sim \ln(T^2/\Phi)$  at different phase transformed fraction of  $Al_{0.25}CoCrFeNi$  high-entropy alloy.

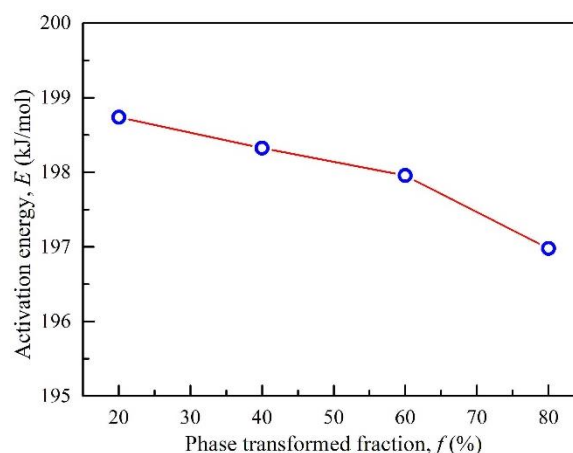


**Figure 5.** Variation of activation energy at different phase transformed fraction of  $Al_{0.25}CoCrFeNi$  high-entropy alloy.

### 3.4. Calculation of Avrami Exponent

The kinetic exponent, also called Avrami exponent, can be used to speculate phase transition mode. The kinetic exponent can be calculated from the classic Johnson-Mehl-Avrami (JMA) model [30], which can be expressed as:

$$f = 1 - \exp(-Kt^n) \quad (3)$$

where  $n$  is the Avrami exponent,  $f$  is the phase transition volume fraction,  $K$  is a constant and  $t$  is the time. Nevertheless, the JMA equation is only applicable for the isothermal phase transformation process. In the case of continuous heating at constant heating rate, the time  $t$  can be express as:

$$t - t_0 = \frac{T - T_0}{\Phi} \quad (4)$$

where  $T_0$  and  $t$  are the starting temperature and time of phase transition. Then the JMA equation can be extended to non-isothermal condition. By incorporating of Equations (3) and (4), after some mathematic treatment, the kinetic exponent can be obtained by the following equation [31]:

$$n = - \frac{\ln(-\ln(1-f))}{\frac{E}{RT}} \quad (5)$$

Then the kinetic exponent  $n$  can be determined from the slope of the  $\ln(-\ln(1-f))$  vs.  $1/T$  curve. For a real phase transformation, the Avrami exponent  $n$  will change with the transformed volume fraction and the so-called local Avrami exponent are always used to determine the changing kinetic exponent at different transformed volume fraction [31]:

$$n = - \frac{\partial \ln(-\ln(1-f))}{\partial \frac{E}{RT}} \quad (6)$$

Taking the sample measured at 4 K/min as an example, the result of Avrami exponent vs. phase transformation volume fraction is presented in Figure 6. Except for the large value of exponent at the quite early and late stage of phase transition, the kinetic exponent,  $n$ , during the majority phase transition process lies in the range 1.5~1 with a small decreasing trend.

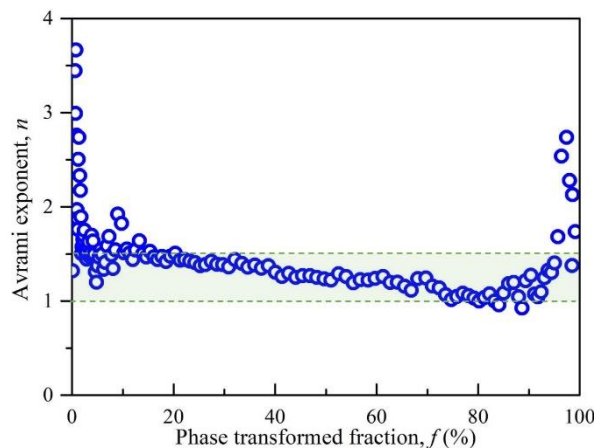


**Figure 6.** The local Avrami exponent (blue circle) as a function of phase transformed fraction of  $\text{Al}_{0.25}\text{CoCrFeNi}$  high-entropy alloy that heated at 4 K/min. The green zone represents the range of  $n$  from 1~1.5.

## 4. Discussion

The  $\text{Al}_{0.25}\text{CoCrFeNi}$  high-entropy alloy is a typical FCC single solid solution alloy. When the as-cast sample was homogenized (1150 °C-24 h), there is a slight difference for the transformation



kinetics, and transformation rate for the homogenized sample is a little bit smaller. As for non-isothermal phase transition process, the phase transition kinetics will be not obviously affected by the homogenization process, especially for  $\text{Al}_{0.25}\text{CoCrFeNi}$  HEA with simple FCC structure. There exists order-disorder phase transition among FCC phase, and the ordered phase is  $\text{L}_{12}$  phase (ordered FCC phase). Figure 7 is the XRD pattern of the alloy that processed just after the finished temperature of the phase transition and as-cast sample. Except a small shift of the lattice parameter, only FCC phase is detected. There is no other new phase formed, and the only phase transition could be the order-disorder phase transition. Many researchers are focus on the phase transition of this alloy. Riva et al. using PXRD to investigate FCC-structured HEAs [32]. By in-situ TEM heating study, Rao et al. [6] found that nano-sized secondary phase precipitated after annealing at 500 °C for  $\text{Al}_{0.3}\text{CoCrFeNi}$  high-entropy alloy, which are not characterized due to the small size of the crystal. By thermal dynamic calculation, they found the phase transition of FCC- $\text{L}_{12}$  and FCC- $\sigma$  could be occurred at this temperature zone and they speculated the secondary phase is  $\sigma$  phase, which is different from the results of Banerjee [25]. In order to clarify the phase transition product, we have checked the microstructure of the sample before and after the phase transition, as shown in Figure 8. It can be seen that, there are precipitates (dark points) with very small size. During heating, the ordered  $\text{L}_{12}$  phase precipitates from the FCC matrix phase as we can found the decreased of the phase from Figure 8b,d. The ordered  $\text{L}_{12}$  precipitates are always coherent with the FCC matrices. The FCC- $\text{L}_{12}$  transition at the studied phase transformation range is an efficient strengthen method to let the FCC HEAs have a good balance between strength and ductility. Thus many researchers are trying to develop the methods that to let the matrix to form the  $\text{L}_{12}$  precipitates as much as possible [33].

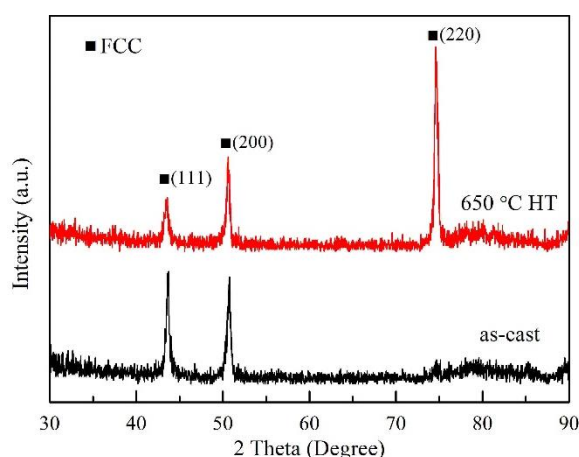


**Figure 7.** The XRD pattern of as cast and heat treated (HT)  $\text{Al}_{0.25}\text{CoCrFeNi}$  high-entropy alloy. The heat treatment procedure is firstly heated to 650 °C at the heating rate of 10 K/min, holding for 1 min and quenched in water.

We can determine the phase transition product from the kinetic parameters. According to the determined kinetic parameters: the activation energy which is rather stable and almost constant during the whole transformation indicating the phase transition is progressed at a constant barrier, and the local environment of the grain nucleation process is very stable. The activation energy determined for FCC  $\text{Al}_{0.25}\text{CoCrFeNi}$  high-entropy alloy is stable with the transformed volume fraction ( $198 \pm 1$  kJ/mol). There are just few results about the kinetic analysis of HEAs, e.g.,  $\text{Al}_{0.5}\text{CoCrFeNi}$  [24], and the activation energy for this alloy is quite different, as the value for the latter will strongly varies with the transformed volume (144–284 kJ/mol). The difference is due to the phase transition type is different, for the latter is FCC-BCC transition while in this study the transition is order-disorder transition. Compared with other metallic materials, actually, there is no specific difference for the absolute value of the activation energy. However, as determined in the paper, the activation energy for this alloy is consistent with transition due to the order-disorder transition which are different from the most phase transformations where activation energy is not constant. What is more,

the calculated kinetic exponent is slight decrease from 1.5 to 1, indicating the whole phase transition process is growth controlled and there is no need for the nucleation process. The order-disorder phase transition is a typical short range diffusion or interface controlled thermal activated growth. During the order-disorder phase transition process, there is no need for the formation of new nuclei, that is to say all the nuclei exist before the transformation process. The above determined kinetic parameters are consistent with the phase transition characteristics of order-disorder phase transition.

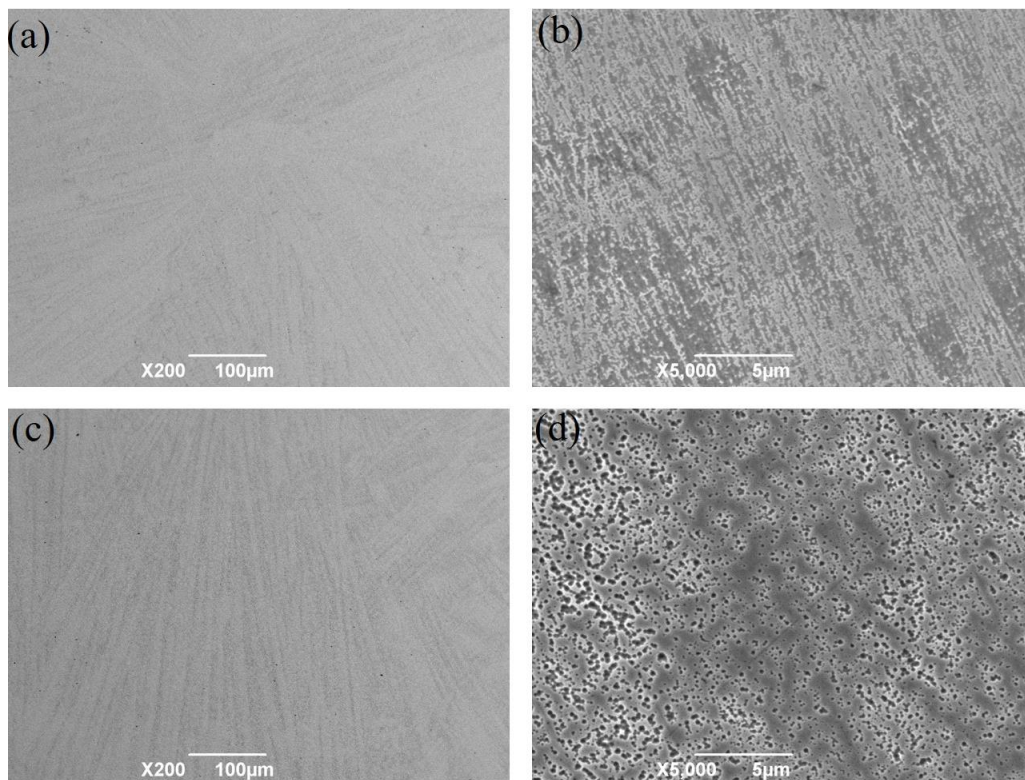


**Figure 8.** The SEM images of as cast (a,b) and heat treated (HT) (c,d)  $\text{Al}_{0.25}\text{CoCrFeNi}$  high-entropy alloy. The heat treatment procedure is firstly heated to 650 °C at the heating rate of 10 K/min, holding for 1 min and quenched in water.

## 5. Conclusions

The thermal expansion experiment of  $\text{Al}_{0.25}\text{CoCrFeNi}$  high-entropy alloy was carried out at different heating rates and the FCC-L1<sub>2</sub> phase transition kinetics was studied. Based on the framework above, the following conclusions are reached:

- (1) The FCC-L1<sub>2</sub> phase transformed fraction as a function of temperature can be determined from the thermal expansion curves using lever rule method.
- (2) The activation energies calculated by KAS formulation at different phase transformed volume are  $198 \pm 1$  kJ/mol, indicating the thermodynamic barrier for the phase transition are independent of the phase transformation process.
- (3) The determined kinetic exponent,  $n$ , shows a decreasing trend from 1.5 to 1 during whole phase transformation process, indicating the phase transition is growth controlled without nucleation process which is the characteristics of order-disorder phase transition.

**Author Contributions:** Conceptualization, J.W.; Investigation: C.W., T.G., H.Y., T.X.; Methodology, T.X., J.W.; Writing-original draft, J.W., C.W., T.X.; Writing-review & editing, J.W., J.L.

**Funding:** This research was funded by the Natural Science Foundation of China (No. and 51774240 and 51571161), and the fund of the State Key Laboratory of Solidification Processing in NWPU (121-TZ-2015).

**Conflicts of Interest:** The authors declare no conflict of interest.

## References

1. Zhang, Y.; Zuo, T.T.; Tang, Z.; Gao, M.C.; Dahmen, K.A.; Liaw, P.K.; Lu, Z.P. Microstructures and properties of high-entropy alloys. *Prog. Mater. Sci.* **2014**, *61*, 1–93. [[CrossRef](#)]
2. Yeh, J.W.; Chen, S.K.; Lin, S.J.; Gan, J.Y.; Chin, T.S.; Shun, T.T.; Tsau, C.H.; Chang, S.Y. Nanostructured High-Entropy Alloys with Multiple Principal Elements: Novel Alloy Design Concepts and Outcomes. *Adv. Eng. Mater.* **2004**, *6*, 299–303. [[CrossRef](#)]
3. Cantor, B.; Chang, I.T.H.; Knight, P.; Vincent, A.J.B. Microstructural development in equiatomic multicomponent alloys. *Mater. Sci. Eng. A* **2004**, *375–377*, 213–218. [[CrossRef](#)]
4. Tsai, M.-H. Physical Properties of High Entropy Alloys. *Entropy* **2013**, *15*, 5338–5345. [[CrossRef](#)]
5. Choi, W.-M.; Jung, S.; Jo, Y.H.; Lee, S.; Lee, B.-J. Design of new face-centered cubic high entropy alloys by thermodynamic calculation. *Met. Mater. Int.* **2017**, *23*, 839–847. [[CrossRef](#)]
6. Rao, J.C.; Diao, H.Y.; Ocelik, V.; Vainchtein, D.; Zhang, C.; Kuo, C.; Tang, Z.; Guo, W.; Poplawsky, J.D.; Zhou, Y.; Liaw, P.K.; de Hosson, J.T.M. Secondary phases in Al<sub>x</sub>CoCrFeNi high-entropy alloys: An in-situ TEM heating study and thermodynamic appraisal. *Acta Mater.* **2017**, *131*, 206–220. [[CrossRef](#)]
7. Yang, T.; Xia, S.; Liu, S.; Wang, C.; Liu, S.; Fang, Y.; Zhang, Y.; Xue, J.; Yan, S.; Wang, Y. Precipitation behavior of Al<sub>x</sub>CoCrFeNi high entropy alloys under ion irradiation. *Sci. Rep.* **2016**, *6*, 32146. [[CrossRef](#)]
8. Munitz, A.; Salhov, S.; Hayun, S.; Frage, N. Heat treatment impacts the micro-structure and mechanical properties of AlCoCrFeNi high entropy alloy. *J. Alloys Compd.* **2016**, *683*, 221–230. [[CrossRef](#)]
9. Chen, B.-R.; Yeh, A.-C.; Yeh, J.-W. Effect of one-step recrystallization on the grain boundary evolution of CoCrFeMnNi high entropy alloy and its subsystems. *Sci. Rep.* **2016**, *6*, 22306. [[CrossRef](#)]
10. Wang, J.; Zhang, Y.; Niu, S.Z.; Wang, W.Y.; Kou, H.C.; Li, J.S.; Wang, S.Q.; Beaugnon, E. Formation of a hexagonal closed-packed phase in Al<sub>0.5</sub>CoCrFeNi high entropy alloy. *MRS Commun.* **2017**, *7*, 879–884. [[CrossRef](#)]
11. Won, J.W.; Kang, M.; Kwon, H.-J.; Lim, K.R.; Seo, S.M.; Na, Y.S. Edge-Cracking Behavior of CoCrFeMnNi High-Entropy Alloy During Hot Rolling. *Met. Mater. Int.* **2018**, *24*, 1432–1437. [[CrossRef](#)]
12. Niu, S.; Kou, H.; Guo, T.; Zhang, Y.; Wang, J.; Li, J. Strengthening of nanoprecipitations in an annealed Al<sub>0.5</sub>CoCrFeNi high entropy alloy. *Mater. Sci. Eng. A* **2016**, *671*, 82–86. [[CrossRef](#)]
13. Liu, F.; Sommer, F.; Bos, C.; Mittemeijer, E.J. Analysis of solid state phase transformation kinetics: Models and recipes. *Int. Mater. Rev.* **2007**, *52*, 193–212. [[CrossRef](#)]
14. Zhang, Y.; Li, J.; Wang, J.; Wang, W.Y.; Kou, H.; Beaugnon, E. Temperature dependent deformation mechanisms of Al<sub>0.3</sub>CoCrFeNi high-entropy alloy, starting from serrated flow behavior. *J. Alloys Compd.* **2018**, *757*, 39–43. [[CrossRef](#)]
15. Wang, J.; Guo, T.; Li, J.; Jia, W.; Kou, H. Microstructure and mechanical properties of non-equilibrium solidified CoCrFeNi high entropy alloy. *Mater. Chem. Phys.* **2018**, *210*, 192–196. [[CrossRef](#)]
16. Guo, T.; Li, J.; Wang, J.; Wang, W.Y.; Liu, Y.; Luo, X.; Kou, H.; Beaugnon, E. Microstructure and properties of bulk Al<sub>0.5</sub>CoCrFeNi high-entropy alloy by cold rolling and subsequent annealing. *Mater. Sci. Eng. A* **2018**, *729*, 141–148. [[CrossRef](#)]
17. Li, M.; Gazquez, J.; Borisevich, A.; Mishra, R.; Flores, K.M. Evaluation of microstructure and mechanical property variations in Al<sub>x</sub>CoCrFeNi high entropy alloys produced by a high-throughput laser deposition method. *Intermetallics* **2018**, *95*, 110–118. [[CrossRef](#)]
18. Joseph, J.; Hodgson, P.; Jarvis, T.; Wu, X.; Stanford, N.; Fabijanic, D.M. Effect of hot isostatic pressing on the microstructure and mechanical properties of additive manufactured Al<sub>x</sub>CoCrFeNi high entropy alloys. *Mater. Sci. Eng. A* **2018**, *733*, 59–70. [[CrossRef](#)]
19. Xia, S.; Gao, M.; Zhang, Y. Abnormal temperature dependence of impact toughness in Al<sub>x</sub>CoCrFeNi system high entropy alloys. *Mater. Chem. Phys.* **2018**, *210*, 213–221. [[CrossRef](#)]
20. Bönisch, M.; Wu, Y.; Sehitoglu, H. Twinning-induced strain hardening in dual-phase FeCoCrNiAl<sub>0.5</sub> at room and cryogenic temperature. *Sci. Rep.* **2018**, *8*, 10663. [[CrossRef](#)]
21. Liu, W.; Yang, T.; Liu, C. Precipitation hardening in CoCrFeNi-based high entropy alloys. *Mater. Chem. Phys.* **2018**, *210*, 2–11. [[CrossRef](#)]
22. Linden, Y.; Pinkas, M.; Munitz, A.; Meshi, L. Long-period antiphase domains and short-range order in a B<sub>2</sub> matrix of the AlCoCrFeNi high-entropy alloy. *Scr. Mater.* **2017**, *139*, 49–52. [[CrossRef](#)]



23. Ghassemali, E.; Sonkusare, R.; Biswas, K.; Gurao, N.P. In-situ study of crack initiation and propagation in a dual phase AlCoCrFeNi high entropy alloy. *J. Alloys Compd.* **2017**, *710*, 539–546. [[CrossRef](#)]
24. Wang, J.; Niu, S.; Guo, T.; Kou, H.; Li, J. The FCC to BCC phase transformation kinetics in an Al<sub>0.5</sub>CoCrFeNi high entropy alloy. *J. Alloys Compd.* **2017**, *710*, 144–150. [[CrossRef](#)]
25. Gwalani, B.; Soni, V.; Choudhuri, D.; Lee, M.; Hwang, J.; Nam, S.; Ryu, H.; Hong, S.H.; Banerjee, R. Stability of ordered L1<sub>2</sub> and B<sub>2</sub> precipitates in face centered cubic based high entropy alloys-Al<sub>0.3</sub>CoFeCrNi and Al<sub>0.3</sub>CuFeCrNi<sub>2</sub>. *Scr. Mater.* **2016**, *123*, 130–134. [[CrossRef](#)]
26. Liu, Y.C.; Sommer, F.; Mittemeijer, E.J. Calibration of the differential dilatometric measurement signal upon heating and cooling; thermal expansion of pure iron. *Thermochim. Acta* **2004**, *413*, 215–225. [[CrossRef](#)]
27. Mittemeijer, E.J. *Fundamentals of Materials Science*; Springer: Heidelberg, Germany, 2010; pp. 448–457.
28. Liu, Y.; Liu, C.; Sommer, F.; Mittemeijer, E.J. Martensite formation kinetics of substitutional Fe–0.7at.%Al alloy under uniaxial compressive stress. *Acta Mater.* **2015**, *98*, 164–174. [[CrossRef](#)]
29. Burnham, A.; Dinh, L. A comparison of isoconversional and model-fitting approaches to kinetic parameter estimation and application predictions. *J. Therm. Anal. Calorim.* **2007**, *89*, 479–490. [[CrossRef](#)]
30. Michaelson, C.; Dahms, M. On the determination of nucleation and growth kinetics by calorimetry. *Thermochim. Acta* **1996**, *288*, 9–27. [[CrossRef](#)]
31. Xiang, Z.; Wang, T.; Ma, S.; Qian, L.; Luo, Z.; Song, Y.; Yang, H.; Lu, W. Microstructural evolution and phase transformation kinetics of MnBi alloys. *J. Alloys Compd.* **2018**, *741*, 951–956. [[CrossRef](#)]
32. Riva, S.; Mehraban, S.; Lavery, N.; Schwarzmüller, S.; Oeckler, O.; Brown, S.; Yuseenko, K. The effect of scandium ternary intergrain precipitates in Al-containing high-entropy alloys. *Entropy* **2018**, *20*, 488. [[CrossRef](#)]
33. Liang, Y.-J.; Wang, L.; Wen, Y.; Cheng, B.; Wu, Q.; Cao, T.; Xiao, Q.; Xue, Y.; Sha, G.; Wang, Y. High-content ductile coherent nanoprecipitates achieve ultrastrong high-entropy alloys. *Nat. Commun.* **2018**, *9*, 4063. [[CrossRef](#)] [[PubMed](#)]



© 2018 by the authors. Licensee MDPI, Basel, Switzerland. This article is an open access article distributed under the terms and conditions of the Creative Commons Attribution (CC BY) license (<http://creativecommons.org/licenses/by/4.0/>).